

# Simultaneous sub-second hyperpolarization of the nuclear and electron spins of phosphorus in silicon by optical pumping of exciton transitions

A. Yang,<sup>1</sup> M. Steger,<sup>1</sup> T. Sekiguchi,<sup>1</sup> M. L. W. Thewalt,<sup>1,\*</sup> T. D. Ladd,<sup>2</sup>  
K. M. Itoh,<sup>3</sup> H. Riemann,<sup>4</sup> N. V. Abrosimov,<sup>4</sup> P. Becker,<sup>5</sup> and H.-J. Pohl<sup>6</sup>

<sup>1</sup>*Department of Physics, Simon Fraser University, Burnaby, British Columbia, Canada V5A 1S6*

<sup>2</sup>*E. L. Ginzton Laboratory, Stanford University, Stanford CA 94305, USA*

<sup>3</sup>*Keio University, Yokohama 223-8522, Japan*

<sup>4</sup>*Institute for Crystal Growth (IKZ), 12489 Berlin, Germany*

<sup>5</sup>*PTB Braunschweig, 38116 Braunschweig, Germany*

<sup>6</sup>*VITCON Projectconsult GmbH, 07745 Jena, Germany*

(Dated: Accepted for publication in Physical Review Letters on June 03, 2009)

We demonstrate a method which can hyperpolarize both the electron and nuclear spins of  $^{31}\text{P}$  donors in Si at low field, where both would be essentially unpolarized in equilibrium. It is based on the selective ionization of donors in a specific hyperfine state by optically pumping donor bound exciton hyperfine transitions, which can be spectrally resolved in  $^{28}\text{Si}$ . Electron and nuclear polarizations of 90% and 76%, respectively, are obtained in less than a second, providing an initialization mechanism for qubits based on these spins, and enabling further ESR and NMR studies on dilute  $^{31}\text{P}$  in  $^{28}\text{Si}$ .

Enriched  $^{28}\text{Si}$  is the material of choice for silicon-based quantum computing schemes involving electron or nuclear spins [1, 2, 3, 4, 5], since the removal of the  $^{29}\text{Si}$  nuclear spin results in very long coherence times [4, 6, 7, 8]. Several methods for achieving quantum logic with spin states of the shallow neutral donor ( $\text{D}^0$ )  $^{31}\text{P}$  in  $^{28}\text{Si}$  have been proposed [1, 2, 3] and the manipulation of electron and nuclear spin coherences have been demonstrated [4], but unsolved challenges include the measurement of single spins and the initialization, or polarization, of these spins. Fortuitously, the isotopic enrichment of  $^{28}\text{Si}$  has another dramatic effect: the linewidths of many optical transitions are drastically reduced [9, 10, 11, 12, 13], including those involving  $^{31}\text{P}$ . These narrow transitions have been proposed both for measurement of single spins [12, 13, 14] and for preferentially populating specific spin states [12, 13].

Electron and nuclear spin polarization in silicon has been studied for decades [15, 16, 17, 18, 19, 20, 21, 22, 23, 24], but the nuclear polarization obtained to date has typically been less than a few percent, and requires thousands of seconds to establish. Very recently, a  $^{31}\text{P}$  nuclear polarization of 68% has been reported [24] in a high magnetic field, using a variation of a mechanism first proposed in 1959 [17], and demonstrated in InSb in 1963 [18], but the time constant was still a relatively long 150 s. The method demonstrated here works at low magnetic field, and can simultaneously hyperpolarize both the electron and nuclear spins of  $^{31}\text{P}$  in less than a second.

Preliminary attempts to demonstrate this mechanism yielded relatively small electron and nuclear polarizations [25], due to the fact that until now all samples of  $^{28}\text{Si}$  with sufficiently high enrichment to resolve the donor bound exciton ( $\text{D}^0\text{X}$ ) hyperfine transitions were  $p$ -type, with residual boron acceptor concentrations typ-

ically ten times the  $^{31}\text{P}$  concentration. At low temperature all donors were therefore ionized ( $\text{D}^+$ ), precluding the observation of  $\text{D}^0 \rightarrow \text{D}^0\text{X}$  transitions, unless above-gap excitation provided photoneutralization. This need for above-gap excitation has a strong negative effect on the achievable electron and nuclear polarizations, since it acts to equalize the populations in the four  $\text{D}^0$  hyperfine states.

The results presented here were made possible by a newly grown crystal of  $^{28}\text{Si}$  purposely doped with  $^{31}\text{P}$ . This  $n$ -type sample allowed us to study the  $\text{D}^0 \rightarrow \text{D}^0\text{X}$  transitions without requiring any above-gap excitation, resulting in dramatically larger polarizations. An electron polarization of 90% and nuclear polarization of 76% were obtained simultaneously in less than a second, in a magnetic field and temperature regime where the equilibrium electron polarization was only  $\sim 2\%$ , and the nuclear polarization  $\sim 3 \times 10^{-3}\%$ . These large and rapidly produced hyperpolarizations should be sufficient for the initialization of qubits, given the existence of algorithmic cooling techniques, which expend modest qubit resources to quickly boost relatively high initial polarizations above levels sufficient for fault-tolerant operation [26].

The  $n$ -type  $^{28}\text{Si}$  sample central to obtaining these results was produced from the same 99.991% enriched  $^{28}\text{Si}$  as previous [12, 13, 25]  $p$ -type samples, except that during the final floating zone growth of the dislocation-free single crystal,  $^{31}\text{P}$  was introduced using a dilute mixture of  $\text{PH}_3$  in Ar carrier gas. The resulting crystal had a gradient in  $^{31}\text{P}$  concentration, and the present results were obtained from a slice containing  $1 \times 10^{14} \text{ cm}^{-3}$  boron and  $7 \times 10^{14} \text{ cm}^{-3}$  of  $^{31}\text{P}$ . The sample was a disc with (001) faces, 1.5 mm thick and approximately 1 cm in diameter, mounted in a completely strain free manner in a reflecting cavity, and immersed in liquid He. Other aspects of the apparatus and methods have been described previ-

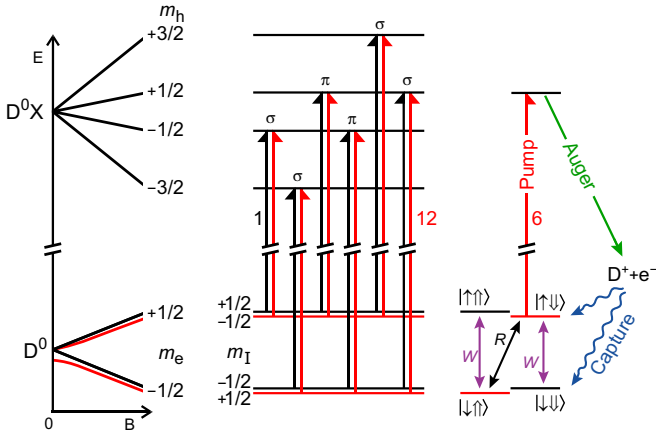


FIG. 1: (Color online) The neutral donor bound exciton transition and its low-field Zeeman splittings are shown, along with a schematic of the selective optical polarization mechanism. On the left are the splittings of the neutral donor ground state ( $D^0$ ) and the bound exciton ground state ( $D^0X$ ). In the centre the twelve allowed optical transitions between the four  $D^0$  hyperfine states and the four  $D^0X$  states are indicated, numbered from 1 to 12 in order of increasing energy. On the right is a simplified schematic of the optical polarization mechanism for the pump laser tuned to line 6.

ously [12, 13, 25]. The optical polarization of the pump and probe lasers do not have a strong influence on the results.

It should be noted that these ultrahigh resolution  $D^0X$  spectra cannot at present be obtained via emission, or PL spectroscopy, the method typically used for studies of  $D^0X$  in semiconductors. The spectral resolution needed to resolve the hyperfine splitting is beyond the capability of available spectrometers. Thanks to tunable, single-frequency lasers, the needed high resolution can be achieved in absorption mode, which we implement using photoluminescence excitation (PLE) spectroscopy.

The Zeeman spectroscopy of  $^{31}\text{P}$  in  $^{28}\text{Si}$  in the low field regime is outlined in FIG. 1. On the left is a sketch of the splittings of the  $D^0$  and  $D^0X$  ground states. The Zeeman splitting of  $D^0X$  is due primarily to the projection of the hole angular momentum ( $m_h$ ), since the two electrons form a spin singlet.  $D^0$  is split at zero magnetic field by the hyperfine interaction into an electron-nuclear singlet and a triplet, separated by 117.53 MHz (486.1 neV) [27]. Under a small magnetic field, these become two hyperfine doublets, each separated by approximately one half of the zero-field splitting. The  $D^0$  hyperfine states consist of two parallel spin states  $|\uparrow\uparrow\rangle$  and  $|\downarrow\downarrow\rangle$  which are not coupled by the hyperfine interaction, and two anti-parallel states  $|\uparrow\downarrow\rangle$  and  $|\downarrow\uparrow\rangle$  which are somewhat mixed by the hyperfine interaction. The dipole allowed  $D^0 \rightarrow D^0X$  transitions are shown in the centre of FIG. 1, numbered from 1 to 12 in order of increasing energy, and consist of six hyperfine-split doublets.

The spectroscopic results are summarized in FIG. 2, beginning at the bottom with the unpumped spectrum of the  $n$ -type sample. This is very similar to previous results [12, 13, 25] for  $p$ -type samples, except that the transitions are slightly less well resolved, with a full width at half-maximum (FWHM) of 220 neV (54 MHz) as compared to 150 neV (37 MHz). Whether this small increase in linewidth is due to concentration broadening from the  $^{31}\text{P}$ , or to an unintentional reduction of the isotopic enrichment, is not known at this time. The populations in the four  $D^0$  hyperfine states are seen to be essentially equal under these conditions, as expected. It is important to note that in order to obtain the spectrum at the bottom of FIG. 2, a small amount of above-gap excitation from a 1047 nm Nd-YLF laser was required in addition to the PLE probe laser. This is not because of a need for photoneutralization, as for  $p$ -type samples, but rather because in the absence of any excitation other than the PLE probe laser, the PLE probe laser itself strongly polarizes the  $D^0$  hyperfine populations. This pumping effect of the probe laser results in a weak and distorted PLE spectrum, but these saturation effects can be circumvented by repopulating the hyperfine states equally with a small amount of above-gap excitation from the 1047 nm laser.

For the other PLE spectra shown in FIG. 2, a much stronger pump laser ( $\sim 2.8 \text{ Wcm}^{-2}$ ) is set to the desired energy while the PLE probe laser ( $\sim 6.5 \times 10^{-2} \text{ Wcm}^{-2}$ ) is scanned across the transitions. For the pumped spectra, no above-gap excitation is used, since now the pump laser holds the populations of the hyperfine states essentially fixed, and any above-gap excitation would merely reduce this desired polarization. Unfortunately, without any above-gap excitation the PLE lines are slightly broadened and develop a low energy tail. This results from Stark broadening due to the  $\sim 1 \times 10^{14} \text{ cm}^{-3}$  of ionized boron and phosphorus which are present in the absence of above-gap excitation. This broadening could be made negligible in a sample with a lower concentration of boron.

The dramatic effects of selective pumping on the  $D^0$  hyperfine populations are immediately apparent in comparing the middle two spectra of FIG. 2 to the unpumped spectrum. The results for pumping line 6 and 8 are shown since these produce the largest, and opposite, polarizations. The resulting electronic polarization is extremely high, with transitions from  $D^0$  states having the same electron spin as the pumped state almost vanishing from the spectra. A large nuclear polarization in the hyperfine doublets from the opposite electron spin states is also apparent. Identical results, except of course for the energies of the transitions, were obtained when the magnetic field was doubled and quadrupled. The top spectrum of FIG. 2 shows the result when the pump laser was positioned at the half height point on the high energy side of line 6, referred to as 6'. The results under the conditions

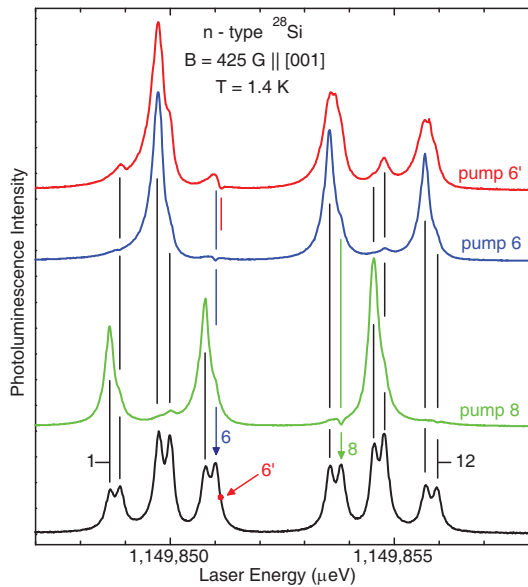


FIG. 2: (Color online) PLE spectra of the  $^{31}\text{P}$  bound exciton in an  $n$ -type  $^{28}\text{Si}$  sample, revealing electron and nuclear polarizations obtained by selective optical pumping. At bottom is a spectrum without any resonant pumping, showing essentially equal populations in the four  $\text{D}^0$  states. The upper spectra show the PLE signal when a strong pump field is tuned to either line 6 or line 8, or the half-height point on the high energy side of line 6, which is indicated as 6'.

of FIG. 2 are summarized in TABLE I, which gives the observed populations of the four  $\text{D}^0$  hyperfine states obtained by curve-fitting to the spectra, and the resulting net electron and nuclear polarizations, when pumping at the peaks of lines 3 through 10 (pumping lines 1, 2, 11 and 12 give results very similar to lines 5, 6, 7 and 8, respectively). Results essentially identical to these were obtained when the pump and probe intensities were both reduced by a factor of one hundred, indicating that high intensity is not needed to obtain high polarization.

The basic mechanism responsible for these polarizations is outlined on the right hand side of FIG. 1 for the case of pumping line 6. Only  $\text{D}^0$  in the  $|\uparrow\downarrow\rangle$  hyperfine state are converted into  $\text{D}^0\text{X}$ , which decay with high probability to ionized donors ( $\text{D}^+$ ) plus free electrons ( $\text{e}^-$ ), due to the dominance of Auger recombination [28] for  $\text{D}^0\text{X}$  in silicon. Subsequent electron capture may then populate the opposite donor electron spin state. The pure nuclear relaxation rate is assumed to be negligible and therefore not shown, and the pump rate is assumed to be much higher than either the optically enhanced electron relaxation rate  $W$ , or the cross relaxation rate  $R$ . Population is therefore removed directly from  $|\uparrow\downarrow\rangle$ , and also from  $|\uparrow\uparrow\rangle$  and  $|\downarrow\uparrow\rangle$ , since these are coupled to  $|\uparrow\downarrow\rangle$  via  $R$  and  $W$  relaxation, and builds up in  $|\downarrow\downarrow\rangle$  to the extent that the effective pump rate exceeds  $W$ . Note that this is very different from earlier mecha-

TABLE I: Observed  $\text{D}^0$  populations and net electron and nuclear polarizations derived from the spectra shown in FIG. 2 and similar spectra for pumping lines 3, 4, 5, 7, 9 and 10.

Pump line	Populations (%)				Polarization(%)	
	$ \uparrow\uparrow\rangle$	$ \uparrow\downarrow\rangle$	$ \downarrow\downarrow\rangle$	$ \downarrow\uparrow\rangle$	Elec.	Nucl.
3 $ \downarrow\downarrow\rangle$	44	38	4	14	64	16
4 $ \downarrow\uparrow\rangle$	63	22	7	8	70	42
5 $ \uparrow\uparrow\rangle$	1	8	75	16	-82	-66
6 $ \uparrow\downarrow\rangle$	1	4	84	11	-90	-76
6' $ \uparrow\downarrow\rangle$	2	11	64	23	-74	-50
7 $ \downarrow\downarrow\rangle$	64	26	1	9	80	46
8 $ \downarrow\uparrow\rangle$	76	18	2	4	88	60
9 $ \uparrow\uparrow\rangle$	3	15	43	39	-64	-16
10 $ \uparrow\downarrow\rangle$	4	5	70	21	-82	-50

nisms of nuclear polarization based on either saturating ESR transitions [15] or on making the  $W$  and  $R$  processes equilibrate at different temperatures [17, 18, 24]. These earlier methods all involve the bidirectional coupling of pairs of states, without or with a Boltzmann factor, respectively, while selective optical pumping can move population unidirectionally from the pumped state to the state having opposite electron spin.

The mechanism limiting the polarization is suggested by several observations. When the pump and probe powers are reduced a factor of 100 the polarizations are essentially unchanged. However when the pump laser is tuned off a peak the polarizations are reduced substantially, as shown for 6' in FIG. 2 and TABLE I. The achievable polarization is therefore likely limited by nonselective photoionization of  $\text{D}^0$  in all four hyperfine states by the pump laser due to the tail of the  $\text{D}^0$  photoionization continuum. Thus even larger hyperpolarizations could be achieved if the substantial inhomogeneous broadening present in this sample could be reduced.

A much more detailed model, incorporating the asymmetric inhomogeneous broadening, the homogeneous linewidth, power broadening, and a dependence on the hole state of the  $\text{D}^0\text{X}$  has been constructed, which can reproduce the details of the spectra, including the spectral hole burning evident at the pump laser energy in the top three spectra in FIG. 2. A full account of the model and the fits to various spectra is beyond the scope of this Letter, but one important result is the fact that, independent of which component of a given hyperfine doublet the pump laser is tuned to, the polarization results are dominated by the coupling to the higher energy, or anti-parallel, component.

To be useful for quantum computing and magnetic resonance, spin polarization must occur on a reasonably fast timescale. Due to the slow detector used in our PLE apparatus, the system cannot capture the electron polarization dynamics, but is still capable of following the time dependence of the nuclear polarization. FIG. 3 shows the transient populations of the four  $\text{D}^0$  hyperfine

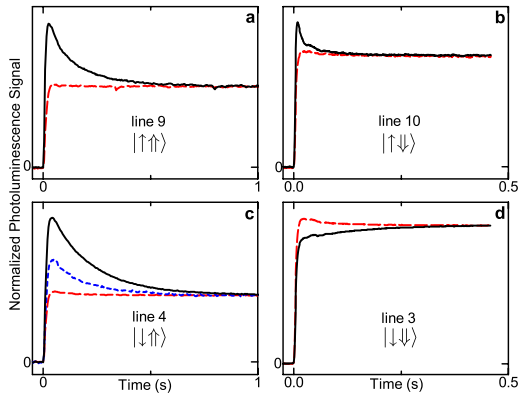


FIG. 3: (Color online) The transient behaviour of lines revealing the four  $D^0$  populations are shown, with the pump laser at line 6 in all cases. Pump and probe are switched on simultaneously at  $t = 0$ . The dashed curves show the transients with the populations in the fully polarized state, while the solid curves show the transients when the populations have been fully equilibrated. The middle curve in **c** shows the transient after the fully polarized sample has recovered in the dark for 20 min.

states with the pump laser on line 6. The transient when pump and probe are turned on simultaneously is shown for both a fully polarized and a fully depolarized initial state. The transient from a polarized initial state is a fast step function, but from the fully depolarized state FIG. 3a, b and c all show an initial overshoot followed by a decay to the steady-state value, due to the transfer of the hyperfine populations to the dominant  $|\downarrow\downarrow\rangle$  state. FIG. 3d shows that the population in the  $|\downarrow\downarrow\rangle$  state, on the other hand, has a buildup following the initial fast transient, with a  $\sim 100$  ms time scale. FIG. 3c also shows the transient behaviour for line 4 when the fully saturated sample is allowed to recover in the dark for 20 min. The partial recovery of the unpolarized population indicates that the nuclear spin relaxation time under these conditions is 35 min.

We have commented already on the fundamental difference between selective optical pumping and previous methods used to obtain nuclear hyperpolarization. The hyperfine-resolved  $D^0X$  transitions are also advantageous in being able to measure directly the relative populations in all four hyperfine states, from which any of the net polarizations or their correlations can be determined. ESR measures only the population difference between the  $|\uparrow\uparrow\rangle$  and  $|\downarrow\uparrow\rangle$  states, and between the  $|\uparrow\downarrow\rangle$  and  $|\downarrow\downarrow\rangle$  states, while NMR (which has not yet been feasible for dilute  $^{31}\text{P}$  in Si) measures the population differences between  $|\uparrow\uparrow\rangle$  and  $|\uparrow\downarrow\rangle$ , and between  $|\downarrow\uparrow\rangle$  and  $|\downarrow\downarrow\rangle$  states. In analyzing their ESR data, McCamey *et al.* [24] have assumed that the  $|\uparrow\uparrow\rangle$  vs.  $|\downarrow\uparrow\rangle$  and  $|\uparrow\downarrow\rangle$  vs.  $|\downarrow\downarrow\rangle$  population ratios are characterized by the same temperature, and that this temperature is the lattice temperature. The extent

to which this assumption can be relied upon in the presence of strong optical excitation is unclear.

The rapidly evolving nuclear polarization we observe is sufficiently high to be useful for quantum computing. Our results also suggest that even higher polarizations will be achieved as better samples of  $^{28}\text{Si}$ , with reduced inhomogeneous broadening resulting from both higher isotopic enrichment and reduced boron content, become available. Selective optical pumping may therefore provide a viable initialization scheme for the  $^{31}\text{P}$  nuclear spin as a qubit in  $^{28}\text{Si}$ , and should work equally well for other shallow donors. It should also make possible NMR studies on  $^{31}\text{P}$  in  $^{28}\text{Si}$ , both normal NMR using the hyperpolarization, as well as optically detected NMR, revealing important new information regarding this potential qubit.

This work is supported by the Natural Sciences and Engineering Research Council of Canada (NSERC).

---

\* Electronic address: thewalt@sfu.ca

- [1] B. E. Kane, *Nature* **393**, 133 (1998).
- [2] D. P. Divincenzo, *Fortschr. Phys.* **48**, 771 (2000).
- [3] R. Vrijen *et al.*, *Phys. Rev. A* **62**, 012306 (2000).
- [4] J. J. L. Morton *et al.*, *Nature* **455**, 1085 (2008).
- [5] T. D. Ladd *et al.*, *Phys. Rev. Lett.* **89**, 017901 (2002).
- [6] A. M. Tyryshkin *et al.*, *Phys. Rev. B* **68**, 193207 (2003).
- [7] A. Tyryshkin *et al.*, *J. Chem. Phys.* **124**, 234508 (2006).
- [8] T. D. Ladd *et al.*, *Phys. Rev. B* **71**, 014401 (2005).
- [9] D. Karaiskaj *et al.*, *Phys. Rev. Lett.* **86**, 6010 (2001).
- [10] D. Karaiskaj *et al.*, *Phys. Rev. Lett.* **90**, 186402 (2003).
- [11] M. L. W. Thewalt *et al.*, *Physica B* **401–402**, 587 (2007).
- [12] A. Yang *et al.*, *Phys. Rev. Lett.* **97**, 227401 (2006).
- [13] M. L. W. Thewalt *et al.*, *J. Appl. Phys.* **101**, 081724 (2007).
- [14] K.-M. C. Fu *et al.*, *Phys. Rev. B* **69**, 125306 (2004).
- [15] G. Feher and E. A. Gere, *Phys. Rev.* **103**, 501 (1956).
- [16] A. Abragam, J. Combrisson, and I. Solomon, *C. R. Acad. Sc. Paris* **246**, 1035 (1958).
- [17] G. Feher, *Phys. Rev. Lett.* **3**, 135 (1959).
- [18] W. G. Clark and G. Feher, *Phys. Rev. Lett.* **10**, 134 (1963).
- [19] G. Lampel, *Phys. Rev. Lett.* **20**, 491 (1968).
- [20] N. T. Bagraev and L. S. Vlasenko, *Sov. Phys. Solid State* **24**, 1974 (1982).
- [21] A. S. Verhulst *et al.*, *Phys. Rev. B* **71**, 235206 (2005).
- [22] H. Hayashi *et al.*, *Phys. Status Solidi c* **3**, 4388 (2006).
- [23] L. S. Vlasenko *et al.*, *Phys. Status Solidi c* **3**, 4376 (2006).
- [24] D. R. McCamey *et al.*, *Phys. Rev. Lett.* **102**, 027601 (2009).
- [25] A. Yang *et al.*, ICPS-29 (Rio de Janeiro, 2008, to be published in the AIP Conf. Proc. Series) (2009).
- [26] L. J. Schulman, T. Mor, and Y. Weinstein, *Phys. Rev. Lett.* **94**, 120501 (2005).
- [27] G. Feher, *Phys. Rev.* **114**, 1219 (1959).
- [28] W. Schmid, *Phys. Status Solidi b* **84**, 529 (1977).